Measurements of Radial Heat Wave Propagation in Laser-Produced Exploding-Foil Plasmas

D. S. Montgomery,[1] O. L. Landen,[1,3] R. P. Drake,[2,3] K. G. Estabrook,[1] H. A. Baldis,[1] S. H. Batha,[2] K. S. Bradley,[3] and R. J. Procassini[1]

[1]*Lawrence Livermore National Laboratory, Livermore, California 94551*
[2]*Plasma Physics Research Institute, University of California Davis and Lawrence Livermore National Laboratory, Livermore, California 94551*
[3]*Department of Applied Science, University of California Davis, Davis, California 95616*

(Received 31 August 1992)

Time-resolved, 2D images of x-ray emission from thin, laser-irradiated titanium foils are presented. The foils are irradiated with 0.35 μm light at intensities of 1×10^{15} W/cm^2 which produces a plasma with electron densities $\leq 10^{22}$ cm^{-3} and electron temperature of 3–4 keV. X-ray emission that is characteristic of the thermal heat front is observed to propagate radially outward from the heated region. Comparison of these measurements with 2D hydrodynamic simulations of the experiment suggests the radial heat flux to be about 3% of the free-streaming heat flux.

PACS numbers: 52.50.Jm, 52.25.Fi, 52.25.Nr

Thermal transport in many-body systems is an important basic topic in physics and becomes difficult when the temperature gradients are steep on the spatial scale of the interactions that limit the heat flow. In this case fluid treatments of the heat transport such as the Spitzer and Härm [1], using transport coefficients derived from local, pertubative kinetic theory, fail to apply and more complicated models must be developed. In the case of nonmagnetically-confined plasmas, such models [2–6] at minimum involve solutions of the Fokker-Planck equation to account for Coulomb collisions, but local magnetic fields, ion-acoustic turbulence, or other effects may also play a role. This topic is also of practical interest since calculations related to laser fusion and other laser-plasma applications must accurately model heat transport. Experimental data are needed to test and refine the models, but it is challenging to perform such experiments, particularly for laser plasmas, with their sub-mm spatial scales and subnanosecond time scales. Steep temperature or density gradients may exist either along the laser axis or radially outward (transverse) from the laser and introduces the complication of heat transport in at least two dimensions. Experiments that specifically address radial heat transport are important for understanding planar target experiments, x-ray laser design, and plasma smoothing of laser inhomogeneties, and the data provide understanding of heat transport in general. While some experiments using preformed plasmas have produced data that could test heat transport models in steep gradients [7,8], progress in laser-produced plasmas has been limited. The heat transport in such plasmas is time and space dependent. However, early heat-transport experiments could only produce time-integrated measurements of absorption, ablated mass, and x-ray emission [9–11]. Later experiments include improvements by using time- and space-resolved measurements of various observables [12–18] but still allowed only complex and model-dependent inferences regarding the thermal heat front motion.

We report the first direct observation of the location and movement of a radially propagating heat front in a laser-produced plasma. The heat front is driven by a heat source of roughly constant temperature, produced using several 0.35 μm laser beams to create a plasma whose central region is underdense to the laser light. The surrounding region is much colder and is overdense, with steep temperature and density gradients. The resulting heat front is directly detected by its distinctive, ringlike x-ray emission as described below. The experimental data are presented and compared to results of a 2D hydrodynamic simulation that uses a simple ("flux-limited") heat-transport model. These data can furthermore be used for comparatively detailed future tests of more sophisticated heat-transport models.

We measure the radial heat wave propagation using a plasma produced by eight beams of the Nova laser [19] irradiating titanium foil targets either 0.5 or 1.5 $\pm$ 0.02 μm thick. Each target is 1.5 $\pm$ 0.1 mm in diameter and is supported on a 1000 Å thick Formvar foil. Each side of the target is illuminated by four beams with 11 $\pm$ 0.5 kJ of 0.35 μm light in a 2 nsec long flat-top laser pulse with 100 psec rising and falling edges. Each of the $f/4.3$ laser beams strikes the target at a 50° angle from the target normal, with its best focus placed 3800 $\pm$ 200 μm in front of the target surface. This produces an effective overlapping spot that is roughly circular and is ~950 μm (FWHM) in diameter. Computer analysis shows the average total intensity is $\sim 1 \times 10^{15}$ W/cm^2 within a 500 μm radius, while the average intensity outside the overlapping region is $\lesssim 1 \times 10^{14}$ W/cm^2 at a radius of 600 μm or greater, dropping rapidly as radius increases.

This experiment allows direct observation of the radial heat front as follows. Initially, x-ray emission from the target dominates within the 500 μm radius laser spot. Later in the laser pulse, the plasma becomes underdense to the laser light in the central 500 μm radius of the foil,

0031-9007/94/73(15)/2055(4)$06.00

and hereafter is called the burnthrough time. The radial density and temperature gradients are steep outside the burnthrough region and define the position of the radial heat front. Within 50 psec after burnthrough, simulations and measurements show that the plasma density within this radius drops to well below $0.5n_{cr}$, where n_{cr} is the critical electron density for 0.35 μm laser light ($n_{cr} \sim 1 \times 10^{22}$ cm^{-3}) and the x-ray emission within this region drops considerably. The calculated electron temperature within the 500 μm radius is 3–4 keV at this time. The plasma density increases rapidly at radii $\gtrsim$ 500 μm, and the temperature decreases at larger radii so that a bright, thin "ring" of x-ray emission is produced. This emission results because the density and temperature gradients at the heat front are opposed and the total x-ray emission from the plasma is proportional to $n_e^2 T_e^\alpha$, where n_e and T_e are the electron density and temperature and α is of order 1.0 [20]. Time-resolved measurements of this emission ring directly show the propagation of the radial heat wave. The temperature-gradient scale length at the heat front may also be estimated from the x-ray emission profile since the emission at the ring decreases linearly with decreasing temperature. We will discuss this last point in a future paper.

The x-ray emission is measured normal to the target plane using a pinhole array imaged onto a strip line, microchannel plate detector. This instrument [21] provides a sequence of several images on each experiment, each image having a spatial and temporal resolution of 15 μm and 80 psec. Source motion blurring limits the spatial resolution to 30 μm for this experiment. A combination of gold photocathode and beryllium filters limits the detector response for x rays with $h\nu \gtrsim 2.5$ keV. The instrument output is recorded onto film, and the film is digitized. The absolute timing of each frame is $\pm$50 psec, but the relative time between sequential frames is more precise. A sequence of two frames is shown in Fig. 1 for the 1.5 μm thick foil after laser burnthrough. The ring-emission radius is measured for each frame by least-squares fitting a circle through the centroid of the ring and has an uncertainty of $\pm$30 μm.

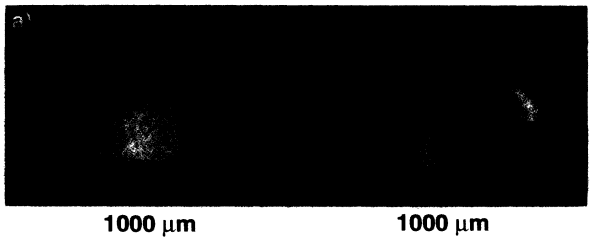

FIG. 1. Time-resolved x-ray images of 1.5 μm foil after laser burnthrough. The frames are at (a) 880 psec and (b) 1030 psec from the beginning of the laser pulse, and the laser burnthrough time is at about 600 psec. The emission ring is superposed over the background plasma emission.

A plot of the ring-emission radius versus time is given in Fig. 2 for both foil thicknesses. The data at a radius ~500 μm are from images where the ring emission first develops. Images at earlier times show a bright emission spot ~500 μm in radius and no indication of any ring structure. These measurements indicate a burnthrough time of about 150 and 600 psec for the 0.5 and 1.5 μm foils. An independent measurement of the burnthrough time for the 1.5 μm foil was made in a separate experiment [22] using a low-intensity 0.53 μm laser probe during the 0.35 μm laser heating beams. This measurement indicates that the plasma becomes transparent to the 0.53 μm laser probe at 600 $\pm$ 50 psec, in excellent agreement with the x-ray measurement. This measurement was not obtained for the 0.5 μm foil.

We performed hydrodynamic simulations of these experiments using the 2D Lagrangian code LASNEX [23]. The modeling used cylindrical coordinates and assumed Z-axis symmetry. The laser wave modeled as a bundle of $f/4.3$ rays in a 50° cone incident on either 0.5 or 1.5 μm titanium foil plus an additional 1000 Å Formvar foil and included a correction for 3D ray paths. The titanium foil radius was 750 μm and the Formvar radius was 1500 μm. An effective laser intensity profile for the overlapping beams was calculated from measurements of a single beam. A calculation of a laser intensity profile with similar focusing as our experiment is described in Ref. [24] and is shown in Fig. 2 of that reference. The calculations use 11 kJ of 0.35 μm light in a 2 nsec trapezoidal pulse on each side of the foil. The calculations include both resonance absorption and linear and nonlinear inverse bremsstrahlung absorption; however, the nonlinear effect [25] is small for our case since $Z(v_{0s}/v_e)^2 \lesssim 0.06$, where Z is the ion charge state and v_{0s}/v_e is the ratio of electron quiver to thermal speeds. Nonlinear inverse bremsstrahlung has negligible effect on the electron distribution at $(2-3)v_e$ compared

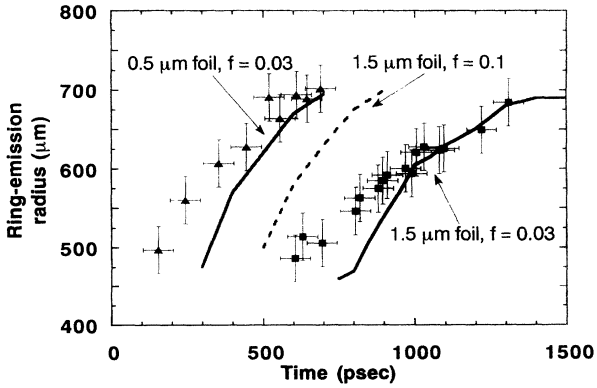

FIG. 2. Plot of the ring-emission radius versus time for the 0.5 μm foil (s) and the 1.5 μm foil (n). The solid-line curves indicate hydrodynamic simulations for each foil thickness using a flux limit $f = 0.03$. The dashed-line curve indicates the simulation for the 1.5 μm foil using a flux limit $f = 0.1$.

to modifications by heat transport itself. At burnthrough time, the calculated absorption is >90% and drops to 30% by 1.5 nsec for the 1.5 μm foil. However, the calculated temperature is roughly constant and drops from 4 to only 3.5 keV during this time. We do not observe significant scattered light from stimulated Raman or stimulated Brillouin scattering, and hot electron production is $\ll 1\%$. We measured a coronal temperature ≥ 3 keV and the peak density evolution, both in good agreement with the simulation results [22], and this gives us confidence in modeling the experiment.

The simulations use multigroup flux-limited heat diffusion, where the heat flux for a given zone is the minimum of the values

$$|Q| = \min[\kappa_{SH} \nabla T_e, f v_e n_e T_e]. \quad (1)$$

The first value in brackets is the classical heat flux where κ_{SH} is the Spitzer and Härm thermal conductivity [1] multiplied by the gradient of the electron temperature ∇T_e. The second value is an expression for the free-streaming heat flux, where v_e is the electron thermal speed and n_e and T_e are the plasma electron density and temperature. The parameter f is the flux-limit value used in the simulations.

We performed simulations using $f = 0.03$ or 0.1 for the 1.5 μm foil and $f = 0.03$ for the 0.5 μm foil. The simulations output the x-ray emissivity for a given radius, integrated along the line of sight of the instrument and take into account radiation transport, opacity, and the response function of the detector. We measured the radius of peak emissivity versus time for each simulation (see Fig. 2). The simulation with $f = 0.03$ is in qualitative agreement with the experiment except that the simulation predicts a slightly later burnthrough time. Simulations with $f = 0.1$ are generally thought to reproduce most of the qualitative features of correct calculations including nonlocal heat transport [26]. The present simulation with $f = 0.1$ yields a burnthrough time which is too early, but more importantly *predicts that the 1.5 μm foil is completely underdense at all radii by 900 psec, in significant disagreement with the experimental observations.* The experiment shows a bright emission ring lasting to 1.5 nsec and longer, whereas the simulation using $f = 0.1$ indicates no such emission past 900 psec since it predicts that the foil is completely heated and underdense at all radii by this time.

Estimates of the electron heat flux into the overdense material and comparison with other heating mechanisms prove useful in understanding the results of the experiment. We estimated the heat flux by examining contour plots of the simulated electron density and temperature. Example plots for the 1.5 μm thick foil at 850 psec are shown in Fig. 3 for $f = 0.03$. The electron temperature is ~ 2 keV at n_{cr} and drops with a scale length of ~ 50 μm. The implied Spitzer and Härm heat flux from Eq. (1) is $\sim 2 \times 10^{15}$ W/cm^2 radially at 600 μm. The flux-limited heat flux from Eq. (1) is $\sim 2 \times 10^{14}$ W/cm^2 for $f = 0.03$.

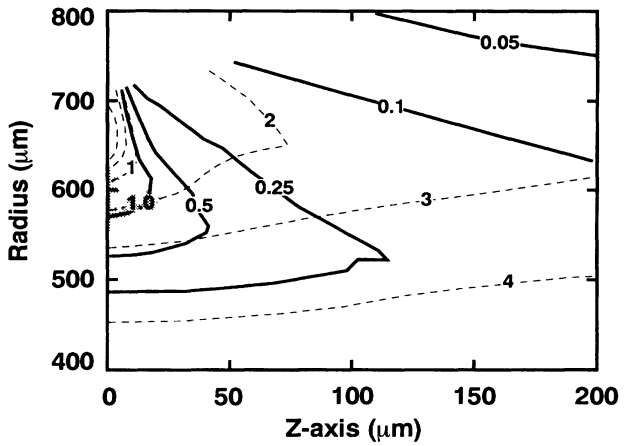

FIG. 3. Contour plots from 2D simulations of the 1.5 μm foil at 850 psec, with a flux limit $f = 0.03$. The solid-line contours are electron density in units of $n_e/n_{cr}(n_{cr} \sim 10^{22}$ cm$^{-3})$. The dashed-line contours are electron temperature (keV). The shaded area indicates the predicted region of strongest thermal-heat flux ($Q > 1.5 \times 10^{14}$ W/cm^2). The predicted ring emission is at $r \cong 570$ μm.

We considered other possible heating mechanisms. Using 2D simulations, we estimated heating by the x-ray flux, suprathermal electrons, compression, and variations in the assumed laser intensity profile. From these calculations we found that thermal electron heat conduction dominates the energy transport to the dense plasma region and that the heat front is driven by the nearly constant temperature underdense plasma. The heat conductivity inferred in the experiment appears to be ~ 10 times lower than one would calculate using Spitzer and Härm conductivity.

The apparent inhibition of heat conduction has been discussed by several authors [2–7,26–29] and has been attributed to such mechanisms as inhibition due to ion-acoustic turbulence, large magnetic fields, and nonlocal transport. Presently, there is no consensus in the literature about the effect of ion-acoustic turbulence on heat transport and will not be discussed in this Letter. We can make crude estimates of magnetic fields and nonlocal transport for these plasmas, but detailed 2D calculations of these effects are nontrivial. A steady-state estimate for a magnetic field generated by density and temperature gradients [29] is given by $B[\mathrm{MG}] \approx 30(T_e)^{1/2}(1/L_T)(A/Z)^{1/2}$, where A and Z are the atomic number and charge state, and L_T is the temperature-gradient scale length in μm. The cross-field heat flux is reduced by $1/[1 + (\omega_{ce}/\nu_{ei})^2]$ where ω_{ce} and ν_{ei} are the electron-cyclotron and electron-ion collision frequencies. A reduction of the heat flux by ~ 10 requires $\omega_{ce}/\nu_{ei} \gtrsim 3$, or $B \gtrsim 2$ MG. We estimate $B \approx 2$ MG for $T_e \approx 2$–3 keV and $A/Z \approx 2$ when $L_T \approx 30$ μm. We performed simulations which included magnetic fields, and regions with $B \approx 2$ MG are produced near the heat front location. However, unrealistically high temperatures (8 keV) are calculated due to

incomplete physics in the magnetohydrodyamics (MHD) model [30] when $\omega_{ce}/\nu_{ei} > 1$, which tends to completely trap the electrons. Microturbulence and 3D effects are not included in the MHD model, and these effects would make the electrons more diffusive and thus lower the electron temperature. Large magnetic fields will affect transport, but present modeling is insufficient to compare to this experiment.

Nonlocal transport becomes important when the mean free path of the heat-carrying electrons, with speeds of $(2-3)v_e$, is comparable to the temperature-gradient scale length. Estimates for the effective "nonlocal" conductivity, based on analytic theory and Fokker-Planck transport calculations, have been published and a crude application of these may be used to determine the role of nonlocal transport in this experiment. A review of two analytic theories compared to Fokker-Planck calculations was published [3] in which the reduced nonlocal conductivity from Fokker-Planck calculations is given as

$$\kappa_{FP}/\kappa_{SH} \approx 1/[1 + 50k\lambda_e], \quad (2)$$

where k is the wave number of the temperature fluctuation and λ_e is the stopping length of the electrons, defined by $\lambda_e = T_e^2/4\pi n_e e^4(Z + 1)^{1/2} \ln\Lambda$, and $\ln\Lambda$ is the Coulomb logarithm. We find λ_e to be 0.5–1.0 μm using $n_e = 10^{22}$ cm^{-3}, $T_e = 2-3$ keV, and $Z = 20$. We approximate $k \approx 2\pi/L_T$ with $L_T \approx 30-50$ μm. Hence, $k\lambda_e \sim 0.1-0.2$ which reduces the conductivity by a factor of 0.09–0.17. A detailed treatment of nonlocal transport is necessary to determine if this is sufficient to explain the experimental observations or if other effects such as magnetic fields are required.

In conclusion, we obtained framed, x-ray images of the emission from laser-heated foils and obtained the first direct observation of a thermal heat front in a laser-plasma. Measurements of the radial propagation of the heat front were made and compared to 2D hydrodynamic simulations which use flux-limited diffusion. We found that a flux limit of 3% of the free-streaming flux is necessary to explain the measurements and is the first time-resolved evidence for strong inhibition of heat flow in the radial direction. Nonlocal heat transport and strong magnetic fields may explain this apparent inhibition in radial heat flow.

The authors acknowledge useful discussions with P. Bell, C. Back, M. Campbell, G. Glendinning, J. Harte, E. Hsieh, R. Kauffman, C. Keane, J. Kilkenny, R. Lee, Y. T. Lee, D. Phillion, M. Rosen, P. Wegner, E. Williams, and G. Zimmerman all from LLNL, and E. M. Epperlein from the University of Rochester. These experiments would not have been possible without the dedicated efforts of the Nova staff. This work was performed under the auspices of the U.S. Department of Energy by LLNL under Contract No. W-7405-ENG-48.

[1] L. Spitzer and R. Härm, Phys. Rev. **89**, 977 (1953).
[2] A. R. Bell, R. G. Evans, and D. J. Nicholas, Phys. Rev. Lett. **46**, 243 (1981).
[3] E. M. Epperlein and R. W. Short, Phys. Fluids B **3**, 3092 (1991).
[4] J. R. Albritton *et al.*, Phys. Rev. Lett. **57**, 1887 (1986).
[5] J. F. Luciani, P. Mora, and J. Virmont, Phys. Rev. Lett. **51**, 1664 (1983).
[6] M. K. Prasad and D. S. Kershaw, Phys. Fluids B **3**, 3087 (1991).
[7] D. R. Gray and J. D. Kilkenny, Plasma Phys. **22**, 81 (1980).
[8] J. H. Rogers *et al.*, Phys. Fluids B **1**, 741 (1989).
[9] R. C. Malone, R. L. McCrory, and R. L. Morse, Phys. Rev. Lett. **34**, 721 (1975).
[10] R. A. Haas *et al.*, Phys. Fluids **20**, 322 (1977).
[11] B. Yaakobi and T. C. Bristow, Phys. Rev. Lett. **38**, 350 (1977).
[12] T. J. Goldsack *et al.*, Phys. Fluids **25**, 1634 (1982).
[13] M. H. Key *et al.*, Phys. Fluids **26**, 2011 (1983).
[14] A. Hauer *et al.*, Phys. Rev. Lett. **53**, 2563 (1984).
[15] P. A. Jaanimagi *et al.*, Appl. Phys. Lett. **38**, 734 (1981).
[16] W. C. Mead *et al.*, Phys. Fluids **27**, 1301 (1984).
[17] C. L. Shepard and P. M. Campbell, Phys. Rev. A **39**, 1344 (1989).
[18] J. W. Murdoch *et al.*, Phys. Fluids **24**, 2107 (1981).
[19] E. M. Campbell *et al.*, Rev. Sci. Instrum. **57**, 2101 (1986).
[20] Y. T. Lee (private communication). Total x-ray emissivity scaling derived from collisional-radiative equilibrium model for ion populations, integrated for $2 < h\nu < 7$ keV, $10^{21} < n_e < 10^{22}$ cm^{-3}, and $1 < T_e < 4$ keV. Model includes free-free, free-bound, and bound-bound emission. Ly-α and He-α lines dominate emission in this region.
[21] P. M. Bell *et al.*, *Ultrahigh Speed and High Speed Photography, Photonics and Videography*, SPIE Proceedings (SPIE–International Society for Optical Engineering, Bellingham, WA, 1990), p. 430.
[22] D. S. Montgomery *et al.*, Bull. Am. Phys. Soc. **36**, 2306 (1991); S. H. Batha *et al.*, (to be published).
[23] G. B. Zimmerman and W. L. Kruer, Comments Plasma Phys. Controlled Fusion **2**, 51 (1975).
[24] S. H. Batha *et al.*, Phys. Fluids B **3**, 2898 (1991).
[25] A. B. Langdon, Phys. Rev. Lett. **44**, 575 (1980).
[26] J. Delettrez, Can. J. Phys. **64**, 932 (1986).
[27] B. H. Ripin *et al.*, Phys. Rev. Lett. **34**, 1313 (1975).
[28] W. M. Manheimer, Phys. Fluids **20**, 265 (1977).
[29] C. E. Max, in *Laser-Plasma Interaction*, edited by R. Balian and J. C. Adam (North-Holland, Amsterdam, 1982).
[30] G. B. Zimmerman (private communication).

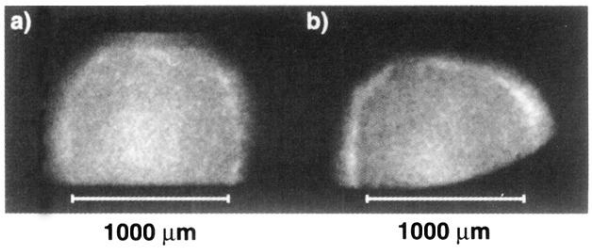

FIG. 1. Time-resolved x-ray images of 1.5 μm foil after laser burnthrough. The frames are at (a) 880 psec and (b) 1030 psec from the beginning of the laser pulse, and the laser burnthrough time is at about 600 psec. The emission ring is superposed over the background plasma emission.

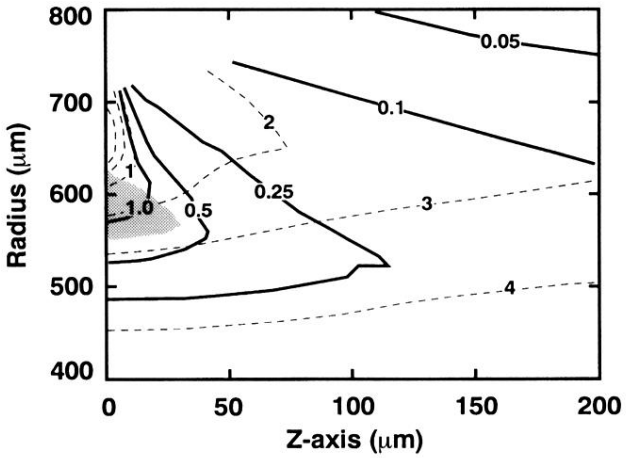

FIG. 3. Contour plots from 2D simulations of the 1.5 μm foil at 850 psec, with a flux limit $f = 0.03$. The solid-line contours are electron density in units of $n_e/n_{cr}(n_{cr} \sim 10^{22}\ cm^{-3})$. The dashed-line contours are electron temperature (keV). The shaded area indicates the predicted region of strongest thermal-heat flux ($Q > 1.5 \times 10^{14}\ W/cm^2$). The predicted ring emission is at $r \cong 570\ \mu$m.